

# HALSIE - Hybrid Approach to Learning Segmentation by Simultaneously Exploiting Image and Event Modalities

Shristi Das Biswas, Adarsh Kosta, Chamika Liyanagedera, Marco Apolinario and Kaushik Roy  
Purdue University, West Lafayette, IN 47907, USA

{sdasbisw, akosta, cliyanag, mapolina, kaushik}@purdue.edu

## Abstract

Standard frame-based algorithms fail to retrieve accurate segmentation maps in challenging real-time applications like autonomous navigation, owing to the limited dynamic range and motion blur prevalent in traditional cameras. Event cameras address these limitations by asynchronously detecting changes in per-pixel intensity to generate event streams with high temporal resolution, high dynamic range, and no motion blur. However, event camera outputs cannot be directly used to generate reliable segmentation maps as they only capture information at the pixels in motion. To augment the missing contextual information, we postulate that fusing spatially dense frames with temporally dense events can generate semantic maps with fine-grained predictions. To this end, we propose HALSIE, a hybrid approach to learning segmentation by simultaneously leveraging image and event modalities. To enable efficient learning across modalities, our proposed hybrid framework comprises two input branches, a Spiking Neural Network (SNN) branch and a standard Artificial Neural Network (ANN) branch to process event and frame data respectively, while exploiting their corresponding neural dynamics. Our hybrid network outperforms the state-of-the-art semantic segmentation benchmarks on DDD17 and MVSEC datasets and shows comparable performance on the DSEC-Semantic dataset with upto  $33.23\times$  reduction in network parameters. Further, our method shows upto  $18.92\times$  improvement in inference cost compared to existing SOTA approaches, making it suitable for resource-constrained edge applications.

## 1. Introduction

There has been a recent paradigm shift in the fields of vision and machine learning to look towards systems that closely mimic biology [1]. The basic apriorism is that biology undergoes temporal evolution to enhance efficiency and adaptability of species. Taking cues from those traits and applying them to modern day Artificial Intelligence (AI) holds considerable prospects for boosting the performance

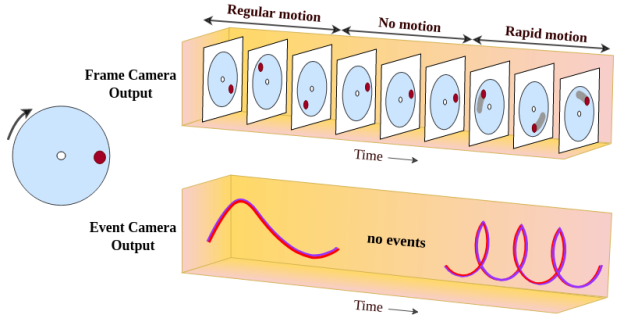


Figure 1. Event cameras asynchronously capture changes in pixel intensities; rate of event generation depends on the speed of motion. Note, no events are generated when there is no motion.

and power efficiency of these systems [2–4].

It is a common sight to see fruit flies executing elaborate foraging missions towards a plate of food put out moments ago, but what escapes us is how they support such complex behaviours with just a million neurons [2, 5] and minimal computational power. Modern AI with significantly higher compute requirements and unlimited resources [6] still fails to replicate the comprehensive real-time scene understanding achieved by these tiny biological systems with their extremely limited power budgets. Present-day AI falls back on conventional video cameras which share little with the biological eye in terms of their scene capturing mechanisms [7] and employ artificial neural networks (ANN) to process the inputs [8–12]. Trying to boost performance of such models often results in subpar memory and power efficiency, and there remains much work to be done before the optimal sweet spot can be found. Re-designing the information processing pipeline right from the data sensors to the algorithms and architectures used for inference can potentially lead to large improvements in energy and efficiency of such systems [13].

Conventional video cameras record motion by sequentially capturing multiple still images each second. They cannot capture any motion between frames. Worse still, each frame repeatedly captures duplicate and irrelevant

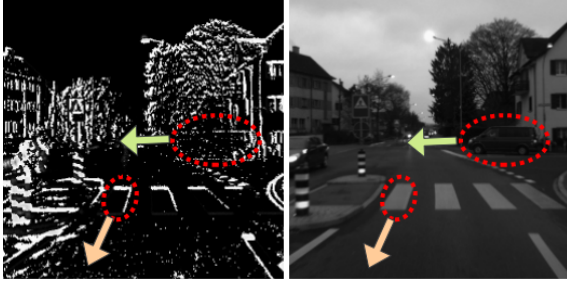


Figure 2. Events capture information only at moving pixels, while lacking the dense spatial information contained in standard frames.

background elements, generating a huge amount of redundant data. Fixed low temporal resolution in standard cameras causes their outputs to suffer from temporal aliasing and motion blur when fast motion is present. High dynamic range scenes captured by frame cameras are further affected because of uneven exposure [14]. Event-cameras, such as Dynamic Vision Sensors (DVS) [15–17] can overcome these issues by asynchronously sampling log intensity changes per-pixel. Such sensors have a higher dynamic range (140dB vs 60dB), higher temporal resolution (10 $\mu$ s vs 3ms), and lower power consumption (10mW vs 3W) compared to frame cameras [14, 18, 19]. However, event cameras generate sparse data streams as they only capture information at moving pixels (Fig. 1). This renders dense pixel-wise predictions from events challenging [20]. As seen in Fig. 2, pixel intensity information is absent at places where events were not recorded leading to scenes with incomplete contextual information. This can be complemented by the dense spatial information from frames. On the other hand, the vehicle captured by a frame camera depicted in Fig. 2 (highlighted in a red circle) is concealed by the immediate background having similar pixel intensity. However, the same vehicle captured by an event-camera shows events at the edges of the vehicle. It is clear that each of the cameras by itself is unable to accurately capture all relevant information in this scene, necessitating a network architecture capable of multi-modal learning [21–23].

However, traditional ANN architectures are inept at directly handling the discrete, asynchronous event streams from an event camera [14]. They perform sub-optimal stateless computations by ignoring the timing information embedded in the data stream. Spiking Neural Networks (SNN) [24], on the other hand, are ideal for event data. They perform asynchronous event-driven computations [25] and offer an implicit recurrence through their internal neuronal state called ‘membrane potential’ to preserve the temporal information in the inputs [26]. Such traits make SNNs ideal for handling sequential inputs efficiently, enabling considerable energy savings when implemented on highly energy-efficient neuromorphic hardware [27–29].

In this work, we present a method for multi-modal learn-

ing from frames and asynchronous event streams for the task of semantic segmentation. Our main contributions are as follows: (1) We propose HALSIE, a deep hybrid SNN-ANN architecture to simultaneously process event streams and frames, leveraging their complementary sensing capabilities. (2) We show how combining events and frames allows better information retrieval from a scene (compared to these modalities working independently), leading to more accurate predictions. (3) We show that our work outperforms the state-of-the-art for semantic segmentation. We evaluate HALSIE on DDD-17 [30], MVSEC [31] and DSEC-Semantic [32] datasets and demonstrate how our proposed method achieves substantial reduction in the network size and inference energy cost.

## 2. Related works

The first work to adapt events for semantic segmentation [33] used an Xception-type network [34] to achieve robust performance in corner case scenes where traditional frames suffer from over-exposure. The authors published the first event-based semantic segmentation dataset with approximate pseudo-labels on some sequences of the DAVIS driving dataset DDD17 [30], generated using a network pretrained on grayscale frames from DAVIS346B [15, 16]. The work by [35] showed improvements over [33] by converting synthetic events from videos and augmenting them to the training dataset. Their method shows considerable boost in performance since they train on real as well as synthetic events. However, it requires video datasets, very few of which exist for semantic segmentation tasks. Improving upon their approach, [36] merged unlabeled events and frames from DAVIS sensors with labeled image datasets such as Cityscapes [37] and reported better performance. In contrast, [38] proposed event-to-image transfer to boost accuracy in semantic segmentation. However, they do not consider any network blocks to address the inherent temporal correlation in events, making their approach similar to how we treat frames. The work by [32] transfers the segmentation task from existing labeled image datasets to unlabeled events via unsupervised domain adaptation (UDA) by aligning recurrent, motion-invariant event embeddings with image embeddings. The authors in [39] convert events to images and process them with standard ANNs, incurring overheads during image generation from events. Instead, [40] reports a UDA method for ‘image-to-event transfer’, that splits the embedding space into motion-specific features shared by both events and images. They align image and event embedding spaces using adversarial learning. However, their method depends on hallucination of motion from still images to generate fake events and is prone to mode collapse [41]. The work in [42] attempts a fully spiking approach using only events for segmentation, but reports poor performance. Our method, HALSIE addresses these

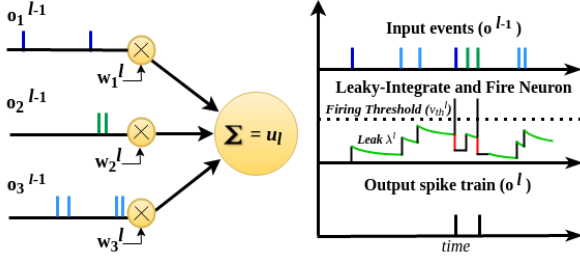


Figure 3. Dynamics of a Leaky-Integrate and Fire (LIF) neuron. The firing threshold  $v_{th}^l$  and the leak factor  $\lambda^l$  are dynamically updated during training to attain best possible performance.

limitations as follows: (i) it brings together complementary sensing capabilities of the event and frame sensors, allowing efficient multi-modal learning, (ii) takes care of the temporal correlation in events by exploiting the inherent recurrence and neuronal dynamics of spiking neural networks for improved performance without additional parametric and learning overheads, and (iii) puts forth a hybrid SNN-ANN architecture to efficiently process events and corresponding frame data with considerable energy savings.

## 3. Method

### 3.1. Multi-modal Learning

Conventional methods [8–12] consider still images as cues, which are not as effective for segmenting objects in videos with high dynamic range or motion blur. Event cameras, on the other hand, sample the log intensity changes at each discrete pixel asynchronously and independently. Any change in the log intensity ( $I$ ) over a specified threshold ( $\theta$ ) is recorded as a discrete event at that pixel location, (i.e.,  $\|\log(I_{t+1}) - \log(I_t)\| \geq \theta$ ), making it ideal for motion capture, especially at high speeds, where traditional cameras suffer from motion blur [14, 18].

Semantic segmentation [43] can be severely affected by the image degradation observed in frame-based camera outputs in challenging environments. Though, event cameras just by themselves are not generally suited for vision applications as they lack precise spatial intensity information, they can assist the learning process by helping the network recognize moving edges in a scene. Frame cameras, on the other hand, provide dense spatial intensity and structural information about the scene, and are essential for capturing stationary objects missed by event-cameras. This motivates the need for an end-to-end multi-modal framework that encodes features from the two modalities into a common latent space to enable richer feature extraction. Additionally, numerous sensors available today, including the Dynamic and Active Vision Sensor (DAVIS) [15, 16], can simultaneously generate asynchronous events and synchronous grayscale frames, reducing the hardware costs of multi-modal data acquisition. Now, both data modalities have a single camera

coordinate system, eliminating the requirements for any expensive transformation and synchronization between multiple coordinate systems. In this work, we combine raw event streams and grayscale images recorded by DAVIS sensors to generate semantic maps with fine grained predictions.

### 3.2. Spiking Neuron Model

The Leaky-Integrate-and-Fire (LIF) [44, 45] is the most widely used bio-inspired neuron model because of its inherent ability to ‘remember’ and ‘recall’ past information without explosion of model parameters over time. Internal dynamics of a LIF neuron model is formulated as follows:

$$u_{mem}^l[t] = w^l o^{l-1}[t] + \lambda^l u_{mem}^l[t-1] - v_{th}^l o^l[t-1] \quad (1)$$

$$\chi[t] = u_{mem}[t] - v_{th} \quad (2)$$

$$o[t] = \mathcal{H}(\chi[t]) \quad (3)$$

where  $u_{mem}^l[t]$  indicates membrane potential of the neuron  $l$  at timestep  $t$  and  $w^l$  are the synaptic weights between neurons  $l-1$  and  $l$ .  $\lambda^l$ ,  $v_{th}^l$  and  $o^l$  are the leak factor, firing threshold and binary output spike of neuron  $l$ , respectively.  $\mathcal{H}$  represents the Heaviside step function [46]. At timestep  $t$ , weighted output spikes from the previous neuron  $l-1$  are accumulated in the membrane potential of the neuron  $l$  creating a ‘short-term memory’. At the same time, the membrane potential of the neuron  $l$  decays by a learned leak factor to represent ‘adaptive forgetting’. Once the accumulated membrane potential exceeds the firing threshold, the neuron will generate a spike at the output ( $o^l$ ). Following spike generation, the membrane potential of the neuron is reset using a ‘soft reset’ mechanism which brings down  $u_{mem}$  by a value equal to the firing threshold ( $v_{th}^l$ ) [47, 48]. A visual representation of the neural dynamics is shown in Fig. 3.

The firing threshold and leak factor for neurons are conventionally considered to be hyper-parameters and determined *a priori* based on neuronal dynamics. We assert that the network dynamically learning the  $v_{th}$  and  $\lambda$  for each layer during training allows for a better search space to find the optimal parameters. In other words, allowing the network to learn how ‘important’ a new input is, or how much of the past experiences should influence its current state, enables deep SNNs to learn more complex tasks [49].

### 3.3. Network Architecture

The proposed HALSIE architecture features a deep hybrid encoder-decoder network to support end-to-end learning. To efficiently extract rich visual features from the inputs, we design a dual-path encoder comprising of an ANN branch for frame inputs and an SNN branch for event inputs, each made up of  $3 \times 3$  convolution layers. The input to the SNN branch is a series of 10 event bins, fed sequentially over 10 timesteps. Event bins are generated by discretizing the input event stream into temporal bins of  $T$  duration or  $k$

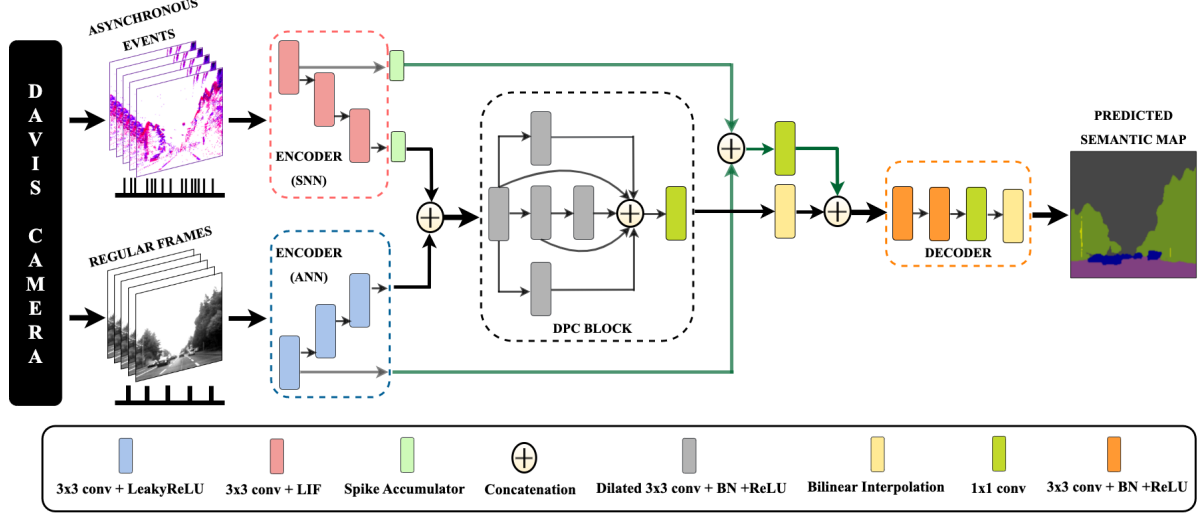


Figure 4. Detailed illustration of the proposed HALSIE framework. The network contains the SNN- and ANN-based encoder branches to extract features from asynchronous event streams and synchronized grayscale images, respectively. Rest of the network, involving the multi-scale processing and decoder blocks, are composed of ANN layers. Best viewed in color.

number of events. The optimum number for  $T$  or  $k$  can depend on the data rate of the sensor or dataset (See Sec. 4 for details). At any timestep  $t$ , LIF neurons in the SNN layer follow the neural dynamics described in Sec. 3.2. Output at a layer  $l$  undergoes spatial decimation using strides (the number of channels are scaled up by a factor of 2) before being forwarded to the next layer as shown in Fig. 4. At every timestep, membrane potentials from the spiking encoder layers are integrated into the corresponding output accumulator. In the ANN encoder-branch, synchronized grayscale image from the DAVIS sensor is passed through the channels of the ANN layers (see Sec. 4). Each ANN block consists of a convolution layer, batch-norm (BN) [50] and a LeakyReLU function [51]. Similar to the SNN branch, intermediate feature maps are downsampled at each ANN layer. The grayscale images temporally closest to the event bins are used as the inputs to the ANN branch. If multiple grayscale images are available over the 10 event bins, they can be fed as separate channels at the input (see Sec. 4).

After forward propagation is completed in both encoders, we perform multi-scale processing. ANN feature maps at the highest-resolution and lowest-resolution scales are concatenated with the corresponding accumulated membrane potentials from the SNN branch to obtain high- and low-resolution fused activations. Next, the low-resolution fused activations from the last encoder layer pass through a Dense Prediction Cell (DPC) [52] with each branch of the cell learning contextual information through parallel or cascaded feature representations and assembling multi-scale context. Dilated convolution [12] used in this block with an output stride=8 helps put space between kernel weights. This increases the size of the receptive field while main-

taining a large spatial resolution of the feature maps at the end of the network, which is necessary to learn fine-grained structure information from the inputs. Multi-scale feature maps from the DPC block and the high-resolution fused activations are passed through  $1 \times 1$  conv layers and then concatenated. The output obtained is passed to an ANN decoder block with a fully-convolutional head consisting of 2  $[(3 \times 3 \text{ conv}) \rightarrow (\text{BN}) \rightarrow (\text{ReLU})]$  blocks followed by a  $(1 \times 1 \text{ conv})$  layer for pixel-wise classification. The generated prediction with  $num-clases$  channels is interpolated to the target image size with bilinear upsampling.

### 3.4. Back-propagation through the network

This work uses a weighted pixel-wise cross entropy loss to examine each pixel individually and compare the class predictions to our one-hot encoded target vector. The next step is to perform backpropagation of the loss gradients with respect to the network parameters. However, unlike ANNs, gradient computation in SNNs is not straightforward. LIF neurons have a spiking mechanism that generate non-differentiable threshold functions. Hence, surrogate gradients must be used to approximate the gradient of the Heaviside step function during backpropagation [53, 54]. We use the inverse tangent surrogate gradient function with width  $\gamma = 100$  (to allow sufficient gradient flow) since it is computationally inexpensive [55].

$$\frac{\partial o^l[t]}{\partial u_{mem}^l[t]} = \frac{\partial \mathcal{H}(\chi[t])}{\partial u_{mem}^l[t]} \approx \frac{1}{1 + \gamma(\chi[t])^2} \quad (4)$$

During the backward pass of the training, we unroll the network in time for all timesteps and the errors  $(\frac{\partial \mathcal{L}}{\partial o^l})$  are Back-

propagated Through Time (BPTT) [56] using surrogate gradients. The weight update is computed as the sum of gradients over each time-step, described as follows:

$$\delta w^l = \sum_t \frac{\partial \mathcal{L}}{\partial o^l[t]} \frac{\partial o^l[t]}{\partial u_{mem}^l[t]} \frac{\partial u_{mem}^l[t]}{\partial w^l} = \sum_t \frac{\partial \mathcal{L}}{\partial o^l[t]} \frac{o^{l-1}[t]}{1 + \gamma(\chi[t])^2} \quad (5)$$

Similarly, the threshold and leak updates are computed as

$$\delta v_{th}^l = \sum_t \frac{\partial \mathcal{L}}{\partial o^l[t]} \frac{\partial o^l[t]}{\partial v_{th}^l} = \sum_t \frac{\partial \mathcal{L}}{\partial o^l[t]} \left( \frac{-o^l[t-1]}{1 + \gamma(\chi[t])^2} \right) \quad (6)$$

$$\delta \lambda^l = \sum_t \frac{\partial \mathcal{L}}{\partial o^l[t]} \frac{\partial o^l[t]}{\partial u_{mem}^l[t]} \frac{\partial u_{mem}^l[t]}{\partial \lambda^l} = \sum_t \frac{\partial \mathcal{L}}{\partial o^l[t]} \frac{u_{mem}^l[t-1]}{1 + \gamma(\chi[t])^2} \quad (7)$$

## 4. Experiments

### 4.1. Results on DDD-17

**Dataset:** We use the publicly available driving scene dataset DDD17 [30], which contains 40 different driving sequences of synchronised grayscale images and event data captured by a DVS camera. The dataset does not provide semantic segmentation labels and hence, we use the pseudo labels provided by [33] using an Xception [34] network pre-trained on Cityscapes [37]. Due to the low resolution of the DAVIS camera, several classes are fused to provide labels for six merged classes. From the provided sequences, this work uses a training set consisting of 15,584 frames and a testing set consisting of 3,584 frames with 6 classes.

**Implementation details:** We use a two-channel event representation of accumulated positive and negative events (integrated over a time interval of  $T = 50ms$ ) to obtain encoded event data as visualised in Fig. 5. We perform random flips and rotations on inputs and crop them to  $192 \times 192$  size images. Each event channel contains 10 such encoded event frames passed sequentially through the network. The intuition behind using a multi-channel representation at each timestep is to allow the network to learn pixel ownership for moving objects (pixels on the same object will move in the same direction, and generate spatially close same polarity events) directly while capturing the short term temporal correlation over timesteps using neuronal dynamics. In the ANN-encoder branch, corresponding frames pass through ANN layers as a 10-channel input. We train our model using the Adam optimizer [57] for 100 epochs with a batch size of 32. The initial learning rate of  $8e-4$  is scaled by 0.7 over epochs. Following past works, we report accuracy and mean intersection over union (mIoU) on our segmentation maps to evaluate performance.

**Qualitative Results:** We evaluate our method on the test set and the quantitative results are shown in Tab. 1 and visualized in Fig. 6. We compare our method with existing methods such as [33, 36, 38, 40] among others, and find that our method using multi-modal learning outperforms

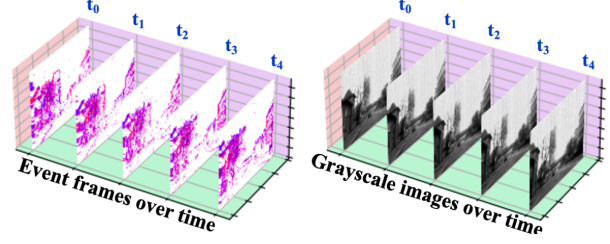


Figure 5. Input event representation. (left) Accumulated event frames, as done in [33], serve as inputs to the SNN-encoder. (right) Corresponding grayscale frames are passed to the ANN-encoder.

the state-of-the-art. Compared to [32], which uses aligned motion-invariant event embeddings and a recurrent event encoder to retain memory over time, our work achieves marginally better performance with a significant 85.9% reduction in network parameters. This can be mainly attributed to the inherent self-recurrence in SNNs, which are more suitable to extract sparse features compared to RNNs, as pointed out in [59]. Using frame information in addition to events allows our method to generate reliable predictions with a lightweight network and around 73% reduced inference cost without compromising on qualitative performance. Our method also shows an 8% increase in mIoU compared to [35], which converts DDD17 grayscale images to synthetic event data and trains on them using DDD17 labels. However, not only do they suffer from a domain gap between synthetic and real events, but also fail to leverage the temporally dense real events to detect finer details in their predictions. In contrast, [42] reconfigured neuronal dynamics of the LIF neurons to include dilated convolutions, while using an energy-efficient fully-spiking network to report results. Their method uses only event data and reports very low performance, in line with our intuition regarding the need for multi-modal hybrid networks to leverage complementary information from both the sensors for improved performance. In the first row in Fig. 6, our segmentation maps were unable to predict the tower peak above the vegetation and classifies it as vegetation itself. However, since the tower peak is not a crucial element in the scene compared to the presence of a nearby traffic pole, an incoming vehicle or person, we posit that the error is not critical. Our method makes more reliable predictions in the scenes in the second and third row compared to its counterparts. For details on how we compute the approximate inference energy for different works, refer to the suppl. material.

### 4.2. Results on MVSEC

**Dataset:** As the events in the DDD17 dataset are very sparse and noisy, we present experimental results on the MVSEC dataset [31] comprising of various driving scenes for stereo estimation. We use ‘outdoor day2’ sequence and divide the data into training and testing sets. We remove

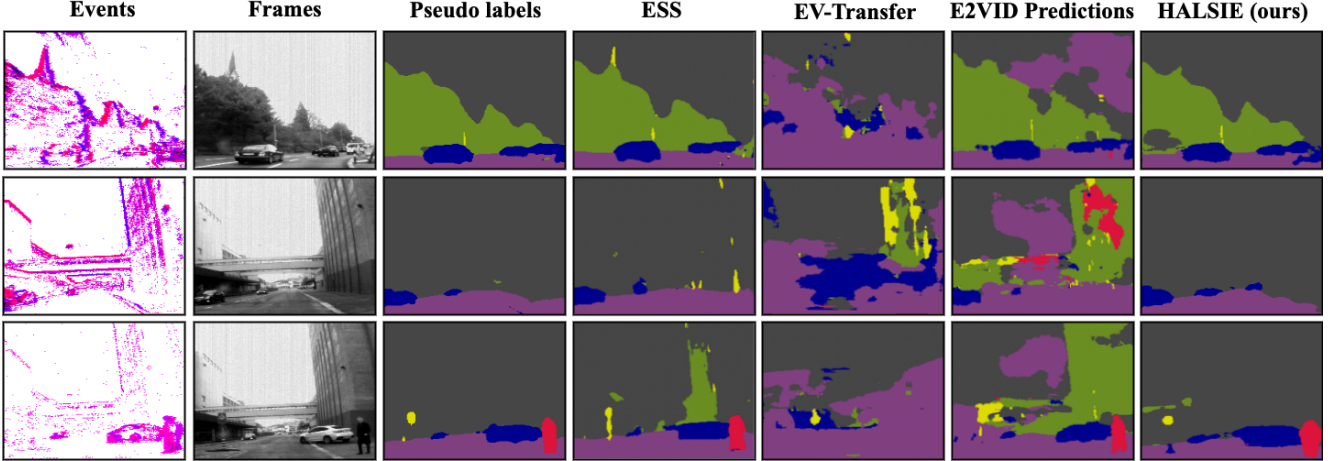


Figure 6. Qualitative results on DDD17 test dataset. Compared to state-of-the-art, our lightweight method is able to generate more reliable predictions with upto 72.65% lower inference energy. Best viewed in color.

Table 1. Quantitative evaluation on the DDD17 dataset, measured by accuracy and mIoU. Comparison of number of parameters and computational energy cost is provided based on standard 45nm CMOS process [58]. Best numbers highlighted in bold.

Method	Accuracy [%]	mIoU [%]	Network	#Parameters( $\times 10^6$ )	#FLOPs <sub>ANN</sub> ( $\times 10^9$ )	#FLOPs <sub>SNN</sub> ( $\times 10^6$ )	E <sub>Total</sub> (mJ)
EV-SegNet [33]	89.76	54.81	ANN	29.09	73.62	-	338.65
EvDistill [36]	-	58.02	ANN	59.34	12.45	-	57.27
DTL [38]	-	58.80	ANN	60.48	16.74	-	77.01
Spiking-Deeplab [42]	-	33.70	SNN	4.14	-	$54.338 \times 10^3$	48.91
E2ViD [39]	83.24	44.77	ANN	10.71	16.65	-	76.59
EV-Transfer [40]	47.37	14.91	ANN	7.37	7.88	-	36.25
ViD2E [35]	90.19	56.01	ANN	29.09	73.62	-	338.65
ESS [32]	90.37	60.43	ANN	12.91	14.22	-	65.41
Ours (HALSIE)	<b>92.50</b>	<b>60.66</b>	Hybrid	<b>1.82</b>	<b>3.84</b>	<b>0.267</b>	<b>17.89</b>

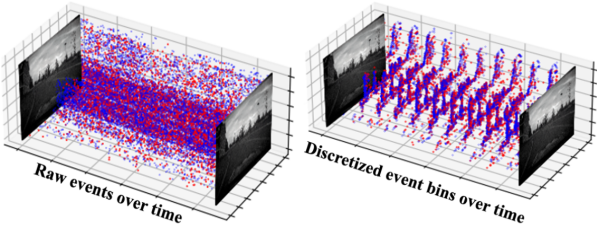


Figure 7. (left) Asynchronous raw event stream between two consecutive frames. (right) Discretized event bins over time.

redundant sequences, such as vehicles stopping at traffic lights, etc. as in past works [36]. As there are no segmentation labels in this dataset, we modulate the pixel intensities of the grayscale frames to make them visually resemble the Cityscapes [37] dataset to our best capability and generate pseudo labels on these frames, similar to [33].

**Implementation details:** As discussed in [20], event data is generated in the Address Event Representation (AER) format of the form  $\{x, y, t, p\}$ , with  $(x, y)$  representing pixel locations,  $(t)$  representing the camera timestamp and  $(p)$  representing the polarity of the intensity change. We use discretized event volume representation similar to [60, 61]. Note that the input representation was varied across datasets

we evaluate on, to best suit the format in which data was released while trying to maintain fidelity with our method. For a set of  $N$  input events  $\{(x_i, y_i, t_i, p_i)\}_{i \in [1, N]}$  between two consecutive grayscale images and a set of  $B$  event bins to be created within this event volume, the discretized event volume is generated using bilinear sampling as follows:

$$t_i^* = (B - 1)(t_i - t_1)/(t_N - t_1) \quad (8)$$

$$V(x, y, t) = \sum_i p_i k_b(x - x_i) k_b(y - y_i) k_b(t - t_i^*) \quad (9)$$

$$k_b = \max[0, 1 - |a|] \quad (10)$$

where  $k_b(a)$  is the bilinear sampling kernel from [62]. We generate 10 such event bins, each having positive and negative polarity channels, to be passed sequentially as timesteps through the network. Pseudo-labels generated on the latter grayscale images in the event window serve as the ground truth for our network. The input representation is visualised in Fig. 7. During training we perform several data augmentation steps including crops, rotations, vertical and horizontal flips. We train our model using the setup described before for 10 epochs using a batch-size of 32.

**Qualitative Results:** The qualitative and quantitative results are shown in Fig. 8 and Tab. 2. We compare our

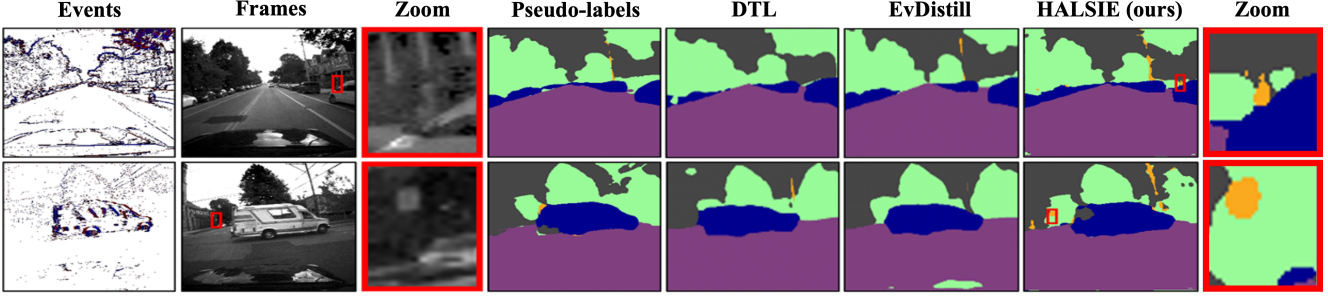


Figure 8. Qualitative results of existing approaches and our method on MVSEC dataset. Due to the low-quality semantic labels, small objects are sometimes missed in the pseudo labels, (zoomed-in image patch in the 3rd column). This leads to a lower detection score on MVSEC even though the predictions of our method provide more fine-grained detections (see 8th column).

Table 2. Quantitative evaluation on the MVSEC dataset. Existing approaches [36] and [38] fail to report their accuracy metrics.

Method	Accuracy [%]	mIoU [%]	$E_{\text{Total}}(mJ)$
EvDistill [36]	-	55.09	101.84
DTL [38]	-	60.82	136.89
Ours (HALSIE)	<b>89.89</b>	<b>64.21</b>	<b>31.39</b>

method with two existing methods, [36] and [38], and find that our method is able to detect much finer details. This work surpasses [38] by around 5.57% increase in mIoU with 30x lower trainable parameters and a 77% reduction in inference energy. Effectiveness of our method can also be verified from Fig. 8 where our segmentation results (7th column) are able to detect very fine details such as a pole or a traffic sign (8th column), where our contemporaries fail. This shows that our method is able to leverage complementary characteristics of frames and events to predict dense semantic maps with fine predictions. In several examples, as observed in Fig. 8, we found that our method predicted objects which were not present in the labels but were clearly visible in the images, degrading our detection score. We also use low-light scenes to show how our method provides reliable performance when grayscale frames are ill-exposed. Our lightweight network is able to efficiently extract information from events and shows promising performance in such challenging conditions. Figure 1 in suppl. material shows the qualitative results.

### 4.3. Results on DSEC-semantic

**Dataset:** We further evaluate our method on a recently released semantic segmentation dataset based on the DSEC [63] dataset. DSEC-semantic [32] contains 8082 training samples and 2809 testing samples from the 53 driving sequences in [63], collected from a variety of urban and rural environments in Switzerland using automotive-grade standard cameras and high-resolution event cameras.

**Implementation details:** Similar to [63], we generate 10 event bins with a constant event density of 100K events/bin

Table 3. Results on DSEC-semantic dataset. Our method shows comparable performance to ESS [32] with around 74% lower inference cost, making it suitable for edge-deployment.

Method	Accuracy [%]	mIoU [%]	$E_{\text{Total}}(mJ)$
EV-Transfer [40]	60.50	23.20	197.48
E2ViD [39]	76.67	40.70	416.99
EV-SegNet [33]	88.61	51.76	1863.83
ESS [32]	<b>89.37</b>	<b>53.29</b>	356.32
Ours (HALSIE)	89.01	52.43	<b>94.41</b>

to be passed sequentially to the network and associate the event bins with pseudo-labels using the provided semantic timestamps. The ANN-encoder is fed with images from the left frame-camera corresponding to the same semantic timestamp as the events. We train for 100 epochs with random flips, rotations and a  $448 \times 448$  crop. The initial learning rate of  $5e-4$  is scaled by a factor of 0.7 over epochs.

**Qualitative Results:** We followed [32] to split DSEC-Semantic into train and test sequences, resulting in a training set of size 4017 and a test set of size 1395 with 11 classes. The quantitative results of our method evaluated on the test set is shown in Tab. 3. We compare our method with [33, 39, 40] and find that HALSIE significantly improves segmentation results and surpasses existing methods with around 1.3% increase in mIoU and upto a significant 95% lower inference cost. Our method marginally falls behind [32] in terms of mIoU, while boasting a noteworthy reduction in compute energy by around 73.5%, making it ideal for energy-efficient edge-applications. See Figure 2 in the suppl. material for qualitative samples from our method.

### 4.4. Ablation studies

#### 4.4.1 Sensor fusion

In this section we investigate the effect of sensor fusion in contrast to using just frame-based images or event streams as inputs. We do this by detaching one of the two encoder branches and evaluating the performance of the network. Rows 1,2 and 5 in Tab. 4 highlight results for the single sen-

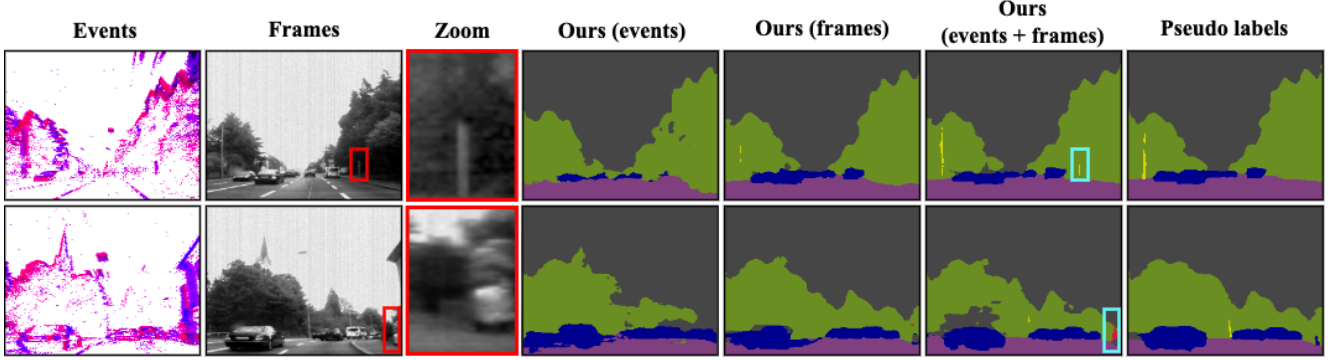


Figure 9. Predictions of our method trained purely with events or frames and our original method trained with both modalities. Finer objects missing from the low-quality pseudo-labels (zoomed-in patch in the red box) are detected by our method trained using events+frames.

Table 4. Ablation results on DDD-17 to study performance on the single-sensor vs. multi-sensor approach.

Method	Training Data	Accuracy [%]	mIoU [%]	#Parameters [ $\times 10^6$ ]
w/o SNN encoder	events	85.99	49.09	1.62
w/o ANN encoder	frames	88.46	56.29	1.62
w/o SNN encoder (iso)	events	87.72	51.13	1.83
w/o ANN encoder (iso)	frames	89.03	57.85	1.83
<b>HALSIE (ours)</b>	<b>events + frames</b>	<b>92.50</b>	<b>60.66</b>	<b>1.82</b>

sensor vs. multi-sensor approaches, where we find that multi-modal inputs achieves better mIoU and accuracy compared to single-sensor inputs. To confirm that the performance improvement in the multi-sensor approach cannot be attributed to increased model capacity (due to two encoder pathways) compared to the single-sensor cases, we try our best to iso-parameterize all the models while maintaining the same network shape. We summarise the results in Rows 3-4 and were able to confirm the validity of our claim. Unsurprisingly, when trained with both the modalities, we can detect small objects like a traffic pole or a person as seen in Fig. 9. In several examples, we find that that our method is able to segment objects that were not present in the labels, but were clearly visible in the images. Fig. 9 shows that our method provides more accurate predictions compared to the pseudo-labels from DDD17 [30] in some cases.

#### 4.4.2 Event representation and event density

We look into the effect of event representation and event density on segmentation performance. For convenience, we mainly focus on experiments on the DSEC-Semantic dataset. Ablation results are shown in Tab. 5 and visualised in Fig. 10. We found that maintaining a moderately dense event bin with constant density shows better segmentation performance compared to high density bins with trailing artifact events from fast moving objects, or low density bins with minimal contribution to the segmentation performance. We also find that having a constant event density consistently performs better than experiments with constant integration time, i.e. a constant event density voxel helps

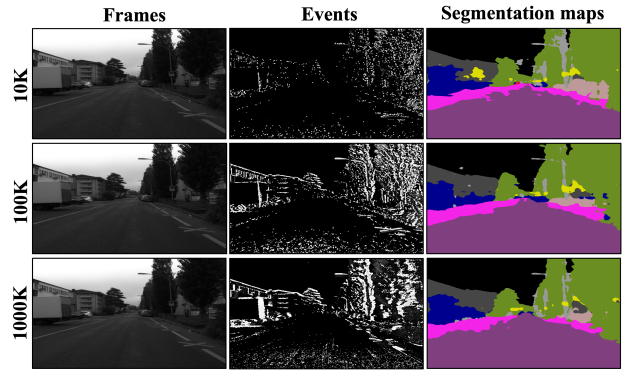


Figure 10. Impact of event window density (top: 10K; middle: 100K; bottom: 1000K) on generated segmentation maps.

Table 5. Ablation experiments on DSEC-Semantic to study the impact of event representation and event bin density.

Event Representation	Constant Event density			Constant Integration Interval		
	10k	100k	1000K	10ms	50ms	100ms
Accuracy [%]	88.78	89.01	88.24	87.76	88.02	87.23
mIoU [%]	51.58	52.43	51.01	50.14	50.67	49.89

the network learn the end-task better.

## 5. Conclusion

We present a simple yet novel hybrid multi-modal framework for predicting segmentation maps in challenging environments. We leverage the complementary characteristics of frame and event-based sensors as well as an ANN-SNN fused architecture leading to potent representations of the latent space, evidenced by the strong performance of our work in detecting finer details on the existing DDD17 and MVSEC benchmarks, and the newly released DSEC-Semantic benchmark. Our work reports state-of-the-art end-task prediction results, while significantly reducing network parameters and computational energy cost, desirable for edge-applications on resource-constrained hardware.

## References

- [1] Y. Zhu, T. Gao, L. Fan, S. Huang, M. Edmonds, H. Liu, F. Gao, C. Zhang, S. Qi, Y. N. Wu, *et al.*, “Dark, beyond deep: A paradigm shift to cognitive ai with humanlike common sense,” *Engineering*, vol. 6, no. 3, pp. 310–345, 2020. **1**
- [2] A. Borst, J. Haag, and D. F. Reiff, “Fly motion vision,” *Annual review of neuroscience*, vol. 33, pp. 49–70, 2010. **1**
- [3] M. Srinivasan, S. Zhang, M. Lehrer, and T. Collett, “Honeybee navigation en route to the goal: visual flight control and odometry,” *Journal of Experimental Biology*, vol. 199, no. 1, pp. 237–244, 1996. **1**
- [4] E. Baird, N. Boeddeker, M. R. Ibbotson, and M. V. Srinivasan, “A universal strategy for visually guided landing,” *Proceedings of the National Academy of Sciences*, vol. 110, no. 46, pp. 18686–18691, 2013. **1**
- [5] L. K. Scheffer, C. S. Xu, M. Januszewski, Z. Lu, S.-y. Takemura, K. J. Hayworth, G. B. Huang, K. Shinomiya, J. Maitlin-Shepard, S. Berg, *et al.*, “A connectome and analysis of the adult drosophila central brain,” *Elife*, vol. 9, 2020. **1**
- [6] V. Sze, Y.-H. Chen, T.-J. Yang, and J. S. Emer, “Efficient processing of deep neural networks: A tutorial and survey,” *Proceedings of the IEEE*, vol. 105, no. 12, pp. 2295–2329, 2017. **1**
- [7] G. J. Lee, C. Choi, D.-H. Kim, and Y. M. Song, “Bioinspired artificial eyes: optic components, digital cameras, and visual prostheses,” *Advanced Functional Materials*, vol. 28, no. 24, p. 1705202, 2018. **1**
- [8] A. Tao, K. Sapra, and B. Catanzaro, “Hierarchical multi-scale attention for semantic segmentation,” *arXiv preprint arXiv:2005.10821*, 2020. **1, 3**
- [9] Y. Yuan, X. Chen, X. Chen, and J. Wang, “Segmentation transformer: Object-contextual representations for semantic segmentation,” *arXiv preprint arXiv:1909.11065*, 2019. **1, 3**
- [10] Y. Yuan, L. Huang, J. Guo, C. Zhang, X. Chen, and J. Wang, “Ocnet: Object context for semantic segmentation,” *International Journal of Computer Vision*, vol. 129, no. 8, pp. 2375–2398, 2021. **1, 3**
- [11] H. Zhao, J. Shi, X. Qi, X. Wang, and J. Jia, “Pyramid scene parsing network,” in *Proceedings of the IEEE conference on computer vision and pattern recognition*, pp. 2881–2890, 2017. **1, 3**
- [12] L.-C. Chen, Y. Zhu, G. Papandreou, F. Schroff, and H. Adam, “Encoder-decoder with atrous separable convolution for semantic image segmentation,” in *Proceedings of the European conference on computer vision (ECCV)*, pp. 801–818, 2018. **1, 3, 4**
- [13] S.-C. Liu and T. Delbruck, “Neuromorphic sensory systems,” *Current opinion in neurobiology*, vol. 20, no. 3, pp. 288–295, 2010. **1**
- [14] G. Gallego, T. Delbrück, G. Orchard, C. Bartolozzi, B. Tabak, A. Censi, S. Leutenegger, A. J. Davison, J. Conradt, K. Daniilidis, *et al.*, “Event-based vision: A survey,” *IEEE transactions on pattern analysis and machine intelligence*, vol. 44, no. 1, pp. 154–180, 2020. **2, 3**
- [15] P. Lichtsteiner, C. Posch, and T. Delbruck, “A  $128 \times 128 \times 120$  db  $15 \mu\text{s}$  latency asynchronous temporal contrast vision sensor,” *IEEE Journal of Solid-State Circuits*, vol. 43, no. 2, pp. 566–576, 2008. **2, 3**
- [16] C. Brandli, R. Berner, M. Yang, S.-C. Liu, and T. Delbruck, “A  $240 \times 180 \times 130$  db  $3 \mu\text{s}$  latency global shutter spatiotemporal vision sensor,” *IEEE Journal of Solid-State Circuits*, vol. 49, no. 10, pp. 2333–2341, 2014. **2, 3**
- [17] T. Delbrück, B. Linares-Barranco, E. Culurciello, and C. Posch, “Activity-driven, event-based vision sensors,” in *Proceedings of 2010 IEEE International Symposium on Circuits and Systems*, pp. 2426–2429, IEEE, 2010. **2**
- [18] A. Lakshmi, A. Chakraborty, and C. S. Thakur, “Neuromorphic vision: From sensors to event-based algorithms,” *Wiley Interdisciplinary Reviews: Data Mining and Knowledge Discovery*, vol. 9, no. 4, p. e1310, 2019. **2, 3**
- [19] M. Mahowald, “The silicon retina,” in *An Analog VLSI System for Stereoscopic Vision*, pp. 4–65, Springer, 1994. **2**
- [20] C. Lee, A. K. Kosta, A. Z. Zhu, K. Chaney, K. Daniilidis, and K. Roy, “Spike-flownet: event-based optical flow estimation with energy-efficient hybrid neural networks,” in *European Conference on Computer Vision*, pp. 366–382, Springer, 2020. **2, 6**
- [21] Y. Huang, C. Du, Z. Xue, X. Chen, H. Zhao, and L. Huang, “What makes multi-modal learning better than single (provably),” *Advances in Neural Information Processing Systems*, vol. 34, pp. 10944–10956, 2021. **2**
- [22] T. Baltrušaitis, C. Ahuja, and L.-P. Morency, “Multimodal machine learning: A survey and taxonomy,” *IEEE Transactions on Pattern Analysis and Machine Intelligence*, vol. 41, no. 2, pp. 423–443, 2019. **2**
- [23] C. Lee, A. K. Kosta, and K. Roy, “Fusion-flownet: Energy-efficient optical flow estimation using sensor fusion and deep fused spiking-analog network architectures,” in *2022 International Conference on Robotics and Automation (ICRA)*, pp. 6504–6510, IEEE, 2022. **2**
- [24] K. Roy, A. Jaiswal, and P. Panda, “Towards spike-based machine intelligence with neuromorphic computing,” *Nature*, vol. 575, no. 7784, pp. 607–617, 2019. **2**
- [25] S. Wang, T. H. Cheng, and M. H. Lim, “A hierarchical taxonomic survey of spiking neural networks,” *Memetic Computing*, vol. 14, no. 3, pp. 335–354, 2022. **2**
- [26] W. Ponghiran and K. Roy, “Spiking neural networks with improved inherent recurrence dynamics for sequential learning,” in *Proceedings of the AAAI Conference on Artificial Intelligence*, vol. 36, pp. 8001–8008, 2022. **2**
- [27] M. Davies, N. Srinivasa, T.-H. Lin, G. Chinya, Y. Cao, S. H. Choday, G. Dimou, P. Joshi, N. Imam, S. Jain, *et al.*, “Loihi: A neuromorphic manycore processor with on-chip learning,” *Ieee Micro*, vol. 38, no. 1, pp. 82–99, 2018. **2**

- [28] F. Akopyan, J. Sawada, A. Cassidy, R. Alvarez-Icaza, J. Arthur, P. Merolla, N. Imam, Y. Nakamura, P. Datta, G.-J. Nam, *et al.*, “Truenorth: Design and tool flow of a 65 mw 1 million neuron programmable neurosynaptic chip,” *IEEE transactions on computer-aided design of integrated circuits and systems*, vol. 34, no. 10, pp. 1537–1557, 2015. [2](#)
- [29] S. B. Furber, F. Galluppi, S. Temple, and L. A. Plana, “The spinnaker project,” *Proceedings of the IEEE*, vol. 102, no. 5, pp. 652–665, 2014. [2](#)
- [30] J. Binas, D. Neil, S.-C. Liu, and T. Delbruck, “Ddd17: End-to-end davis driving dataset,” *arXiv preprint arXiv:1711.01458*, 2017. [2](#), [5](#), [8](#)
- [31] A. Z. Zhu, D. Thakur, T. Özaslan, B. Pfrommer, V. Kumar, and K. Daniilidis, “The multivehicle stereo event camera dataset: An event camera dataset for 3d perception,” *IEEE Robotics and Automation Letters*, vol. 3, no. 3, pp. 2032–2039, 2018. [2](#), [5](#)
- [32] Z. Sun, N. Messikommer, D. Gehrig, and D. Scaramuzza, “Ess: Learning event-based semantic segmentation from still images,” *arXiv preprint arXiv:2203.10016*, 2022. [2](#), [5](#), [6](#), [7](#)
- [33] I. Alonso and A. C. Murillo, “Ev-segnet: Semantic segmentation for event-based cameras,” in *Proceedings of the IEEE/CVF Conference on Computer Vision and Pattern Recognition Workshops*, pp. 0–0, 2019. [2](#), [5](#), [6](#), [7](#)
- [34] F. Chollet, “Xception: Deep learning with depthwise separable convolutions,” in *Proceedings of the IEEE conference on computer vision and pattern recognition*, pp. 1251–1258, 2017. [2](#), [5](#)
- [35] D. Gehrig, M. Gehrig, J. Hidalgo-Carrió, and D. Scaramuzza, “Video to events: Recycling video datasets for event cameras,” in *Proceedings of the IEEE/CVF Conference on Computer Vision and Pattern Recognition*, pp. 3586–3595, 2020. [2](#), [5](#), [6](#)
- [36] L. Wang, Y. Chae, S.-H. Yoon, T.-K. Kim, and K.-J. Yoon, “Evdistill: Asynchronous events to end-task learning via bidirectional reconstruction-guided cross-modal knowledge distillation,” in *Proceedings of the IEEE/CVF Conference on Computer Vision and Pattern Recognition*, pp. 608–619, 2021. [2](#), [5](#), [6](#), [7](#)
- [37] M. Cordts, M. Omran, S. Ramos, T. Rehfeld, M. Enzweiler, R. Benenson, U. Franke, S. Roth, and B. Schiele, “The cityscapes dataset for semantic urban scene understanding,” in *Proceedings of the IEEE conference on computer vision and pattern recognition*, pp. 3213–3223, 2016. [2](#), [5](#), [6](#)
- [38] L. Wang, Y. Chae, and K.-J. Yoon, “Dual transfer learning for event-based end-task prediction via pluggable event to image translation,” in *Proceedings of the IEEE/CVF International Conference on Computer Vision*, pp. 2135–2145, 2021. [2](#), [5](#), [6](#), [7](#)
- [39] H. Rebecq, R. Ranftl, V. Koltun, and D. Scaramuzza, “High speed and high dynamic range video with an event camera,” *IEEE transactions on pattern analysis and machine intelligence*, vol. 43, no. 6, pp. 1964–1980, 2019. [2](#), [6](#), [7](#)
- [40] N. Messikommer, D. Gehrig, M. Gehrig, and D. Scaramuzza, “Bridging the gap between events and frames through unsupervised domain adaptation,” *IEEE Robotics and Automation Letters*, vol. 7, no. 2, pp. 3515–3522, 2022. [2](#), [5](#), [6](#), [7](#)
- [41] H. Thanh-Tung and T. Tran, “Catastrophic forgetting and mode collapse in gans,” in *2020 international joint conference on neural networks (ijcnn)*, pp. 1–10, IEEE, 2020. [2](#)
- [42] Y. Kim, J. Chough, and P. Panda, “Beyond classification: directly training spiking neural networks for semantic segmentation,” *Neuromorphic Computing and Engineering*, 2022. [2](#), [5](#), [6](#)
- [43] M. Thoma, “A survey of semantic segmentation,” *arXiv preprint arXiv:1602.06541*, 2016. [3](#)
- [44] L. F. Abbott, “Lapicque’s introduction of the integrate-and-fire model neuron (1907),” *Brain research bulletin*, vol. 50, no. 5-6, pp. 303–304, 1999. [3](#)
- [45] P. Dayan, L. F. Abbott, *et al.*, “Theoretical neuroscience (vol. 806),” 2001. [3](#)
- [46] E. W. Weisstein, “Heaviside step function,” <https://mathworld.wolfram.com/>, 2002. [3](#)
- [47] E. Ledinauskas, J. Ruseckas, A. Juršėnas, and G. Buračas, “Training deep spiking neural networks,” *arXiv preprint arXiv:2006.04436*, 2020. [3](#)
- [48] B. Han, G. Srinivasan, and K. Roy, “Rmp-snn: Residual membrane potential neuron for enabling deeper high-accuracy and low-latency spiking neural network,” in *Proceedings of the IEEE/CVF conference on computer vision and pattern recognition*, pp. 13558–13567, 2020. [3](#)
- [49] N. Rathi and K. Roy, “Diet-snn: A low-latency spiking neural network with direct input encoding and leakage and threshold optimization,” *IEEE Transactions on Neural Networks and Learning Systems*, 2021. [3](#)
- [50] S. Ioffe and C. Szegedy, “Batch normalization: Accelerating deep network training by reducing internal covariate shift,” in *International conference on machine learning*, pp. 448–456, PMLR, 2015. [4](#)
- [51] B. Xu, N. Wang, T. Chen, and M. Li, “Empirical evaluation of rectified activations in convolutional network,” *arXiv preprint arXiv:1505.00853*, 2015. [4](#)
- [52] L.-C. Chen, M. Collins, Y. Zhu, G. Papandreou, B. Zoph, F. Schroff, H. Adam, and J. Shlens, “Searching for efficient multi-scale architectures for dense image prediction,” *Advances in neural information processing systems*, vol. 31, 2018. [4](#)
- [53] E. O. Neftci, H. Mostafa, and F. Zenke, “Surrogate gradient learning in spiking neural networks: Bringing the power of gradient-based optimization to spiking neural networks,” *IEEE Signal Processing Magazine*, vol. 36, no. 6, pp. 51–63, 2019. [4](#)
- [54] J. H. Lee, T. Delbruck, and M. Pfeiffer, “Training deep spiking neural networks using backpropagation,” *Frontiers in neuroscience*, vol. 10, p. 508, 2016. [4](#)

- [55] J. Hagenaaars, F. Paredes-Vallés, and G. De Croon, “Self-supervised learning of event-based optical flow with spiking neural networks,” *Advances in Neural Information Processing Systems*, vol. 34, pp. 7167–7179, 2021. 4
- [56] P. J. Werbos, “Backpropagation through time: what it does and how to do it,” *Proceedings of the IEEE*, vol. 78, no. 10, pp. 1550–1560, 1990. 5
- [57] D. P. Kingma and J. Ba, “Adam: A method for stochastic optimization,” in *3rd International Conference on Learning Representations, ICLR 2015, San Diego, CA, USA, May 7-9, 2015, Conference Track Proceedings* (Y. Bengio and Y. LeCun, eds.), 2015. 5
- [58] M. Horowitz, “1.1 computing’s energy problem (and what we can do about it),” in *2014 IEEE International Solid-State Circuits Conference Digest of Technical Papers (ISSCC)*, pp. 10–14, 2014. 6
- [59] L. Deng, Y. Wu, X. Hu, L. Liang, Y. Ding, G. Li, G. Zhao, P. Li, and Y. Xie, “Rethinking the performance comparison between snns and anns,” *Neural networks*, vol. 121, pp. 294–307, 2020. 5
- [60] A. Z. Zhu, L. Yuan, K. Chaney, and K. Daniilidis, “Unsupervised event-based learning of optical flow, depth, and egomotion,” in *Proceedings of the IEEE Conference on Computer Vision and Pattern Recognition*, pp. 989–997, 2019. 6
- [61] A. Zihao Zhu, L. Yuan, K. Chaney, and K. Daniilidis, “Unsupervised event-based optical flow using motion compensation,” in *Proceedings of the European Conference on Computer Vision (ECCV) Workshops*, pp. 0–0, 2018. 6
- [62] M. Jaderberg, K. Simonyan, A. Zisserman, and k. kavukcuoglu, “Spatial transformer networks,” in *Advances in Neural Information Processing Systems* (C. Cortes, N. Lawrence, D. Lee, M. Sugiyama, and R. Garnett, eds.), vol. 28, Curran Associates, Inc., 2015. 6
- [63] M. Gehrig, W. Aarents, D. Gehrig, and D. Scaramuzza, “Dsec: A stereo event camera dataset for driving scenarios,” *IEEE Robotics and Automation Letters*, vol. 6, no. 3, pp. 4947–4954, 2021. 7